

000 001 002 003 004 005 LESS IS MORE: IMPROVING MOLECULAR FORCE 006 FIELDS WITH MINIMAL TEMPORAL INFORMATION 007 008 009

010 **Anonymous authors**
011 Paper under double-blind review
012
013
014
015
016
017
018
019
020
021
022
023
024
025
026
027
028
029
030
031
032

ABSTRACT

033 Accurate prediction of energy and forces for 3D molecular systems is one of fundamental challenges at the core of AI for Science applications. Many powerful and data-efficient neural networks predict molecular energies and forces from single atomic configurations. However, one crucial aspect of the data generation process is rarely considered while learning these models i.e. Molecular Dynamics (MD) simulation. Molecular Dynamics (MD) simulations generate time-ordered trajectories of atomic positions that fluctuate in energy and explore regions of the potential energy surface (e.g., under standard NVE/NVT ensembles), rather than being constructed to steadily lower the potential energy toward a minimum as in geometry relaxations. This work explores a novel way to leverage molecular dynamics (MD) data, when available, to improve the performance of such predictors. We introduce a novel training strategy called FRAMES, that use an auxiliary loss function for exploiting the temporal relationships within MD trajectories. Counter-intuitively, on two atomistic benchmarks and a synthetic system we observe that minimal temporal information, captured by pairs of just two consecutive frames, is often sufficient to obtain the best performance, while adding longer trajectory sequences can introduce redundancy and degrade performance. On the widely used MD17 and ISO17 benchmarks, FRAMES significantly outperforms its Equiformer baseline, achieving highly competitive results in both energy and force accuracy. Our work not only presents a novel training strategy which improves the accuracy of the model, but also provides evidence that for distilling physical priors of atomic systems, more temporal data is not always better.

034 1 INTRODUCTION

035 Predicting the quantum properties of atomic systems underpins many tasks in computational chemistry and materials science, yet traditional simulation methods (e.g. ab initio calculations) are often 036 too expensive for large-scale or high-throughput applications. In response, machine learning methods—especially Graph Neural Networks (GNNs) (Wu et al., 2020)—have emerged as a fast and 037 accurate alternative for estimating energies, forces, and other properties, with successful extensions 038 to protein structure prediction, virtual drug screening, and materials design. GNNs generally model 039 atoms as nodes and the physical interaction of two atoms with edges, and also the interaction of 040 atoms with message passing.

041 Among these, *equivariant GNNs*, highly researched in recent years (Finzi et al., 2020; Fuchs et al., 042 2020; Huang et al., 2022; Hutchinson et al., 2021b; Satorras et al., 2021b; Liao & Smidt, 2023), 043 explicitly encode the physical symmetries of space: when the input configuration of atoms is 044 translated, rotated, or reflected, the network’s scalar and vector outputs transform accordingly (Han 045 et al., 2022). By building in these inductive biases, equivariant models achieve greater data efficiency 046 and generalization in single, static atomic configurations—much as convolutional networks do for 047 images. However, nearly all existing equivariant GNNs ignore the rich temporal context information 048 available in the molecular dynamics simulations data they are often trained on.

049 In this work we focus on datasets that explicitly expose Molecular Dynamics (MD) trajectories, 050 i.e., time-ordered configurations sampled at a fixed integration time step under a chosen thermo- 051 dynamic ensemble. This is distinct from geometry relaxations or re-relaxed subsamples (such as 052 revMD17 (Christensen & von Lilienfeld, 2020)), which no longer form a physically meaningful tra- 053

054 trajectory. While many modern MLIP datasets are constructed from a mixture of protocols (equilibrium
 055 databases, rattling, structure searches, etc.), MD-style trajectories remain prevalent and practically
 056 important, for example in large-scale benchmarks with MD-like tasks such as OC20/OC22 (Chanus-
 057 sot et al., 2021; Tran et al., 2023) and follow-up challenges. In this paper we investigate: *when*
 058 *MD trajectories are available, how can we best exploit their temporal structure to improve static*
 059 *predictors with minimal information?*

060 A few recent works have tried to address this by incorporating temporal information, typically by
 061 feeding a fixed sequence of consecutive frames into an equivariant spatio-temporal GNN Wu et al.
 062 (2023); Satorras et al. (2021a). While these approaches can improve trajectory forecasting, they have
 063 two key limitations. First, such models are tied to a fixed history window; they struggle when one
 064 wants to predict a single future frame from an arbitrary state, or when the optimal memory length
 065 varies across the system. Second, they operate on the assumption that more historical data is always
 066 beneficial. This paper challenges that core assumption.

067 In this work, we propose a different approach. Instead of building a complex spatio-temporal model,
 068 we introduce novel training strategy, FRAMES, which utilizes an auxiliary loss function designed
 069 to distill temporal information from MD simulations into a standard predictor. This approach is
 070 model-agnostic and improves the accuracy of any baseline architecture while leaving it purely static
 071 at test time, requiring only a single configuration as input. Furthermore, our framework allows us
 072 to systematically investigate the value of temporal information. We challenge the implicit "more
 073 is better" assumption, hypothesizing that minimal temporal information—derived from just two
 074 consecutive frames—is not only sufficient but optimal. We empirically demonstrate that using more
 075 than two frames can be detrimental, degrading model accuracy and efficiency due to data redundancy.

076 Our contributions are as follows:

- 078 • We introduce FRAMES, a novel training strategy using auxiliary loss that leverages temporal
 079 data from MD trajectories to significantly improve the accuracy of static energy and force
 080 predictors.
- 081 • We provide strong empirical evidence for a "less is more" principle, demonstrating that
 082 using pairs of two consecutive frames is optimal, while performance degrades with three
 083 frames due to data redundancy.
- 084 • Our method, applied to a standard Equiformer (Liao & Smidt, 2023) baseline, achieves
 085 highly competitive results on the MD17 (Chmiela et al., 2017) and ISO17 (Schütt et al.,
 086 2017) benchmarks, validating our approach.

089 2 RELATED WORKS

091 ***SE(3)/E(3)-Equivariant Networks.*** Incorporating $SE(3)/E(3)$ equivariance (equivariance to 3D
 092 rotations, translations, and optionally reflections) as an inductive bias in Graph Neural Networks
 093 (GNNs) is often highly beneficial for modeling 3D atomistic systems, leading to strong data efficiency
 094 and generalization in many benchmarks. At the same time, recent work has shown that carefully
 095 designed non-equivariant or partially equivariant architectures can achieve competitive performance
 096 in some regimes, suggesting a spectrum of effective inductive biases rather than a single universally
 097 superior choice. (Duval et al., 2023) Key approaches include methods based on irreducible repre-
 098 sentations (irreps) of the symmetry group, such as Tensor Field Networks (TFNs) (Thomas et al.,
 099 2018), $SE(3)$ -Transformers (Fuchs et al., 2020), LieTransformer (Hutchinson et al., 2021a), and
 100 Equiformer (Liao & Smidt, 2023) (which FRAMES utilizes). These methods often use spherical
 101 harmonics and tensor products to construct equivariant features and operations. Another significant
 102 line of work involves scalarization or coordinate-based methods, which operate primarily on invariant
 103 quantities (e.g., distances) combined with equivariant directional information. $E(n)$ -Equivariant
 104 Graph Neural Networks (EGNNs) (Satorras et al., 2021a) are a prominent example, offering compu-
 105 tational efficiency by avoiding higher-order representations. (Garcia Satorras et al., 2021) The Graph
 106 Mechanics Network (GMN) (Huang et al., 2022) also employs similar principles for constrained
 107 systems. The field strives for a balance between the expressivity of irrep-based models and the effi-
 108 ciency of scalarization techniques, with attention mechanisms also being integrated into equivariant
 109 frameworks.

108 **Equivariant spatio-temporal graph neural networks.** While most GNNs for molecular dynamics
 109 assume Markovian dynamics (predicting the next state based only on the current one), real systems
 110 exhibit memory effects and periodic motions (Wu et al., 2023). To address this, few equivariant spatio-
 111 temporal GNNs have been developed. These models typically process a sequence of past frames to
 112 predict future states. For instance, ESTAG (Wu et al., 2023) (Equivariant Spatio-Temporal Attentive
 113 Graph Networks) uses historical trajectories and an Equivariant Discrete Fourier Transform (EDFT)
 114 to capture non-Markovian properties and periodic patterns. Equivariant Graph Neural Operator (Xu
 115 et al., 2024) models dynamics as continuous trajectories using equivariant temporal convolutions.
 116 However, such models often rely on a fixed history window at inference, which can be inflexible and
 117 computationally demanding. FRAMES differs by using historical frames to improve the training of
 118 its latent state via a multi-step lookahead loss, while still allowing for efficient single-step inference
 119 without explicit history.
 120

121 **Multi-step Loss and Auxiliary Predictive Objectives.** Auxiliary tasks, where secondary objectives
 122 are learned alongside the primary task, can enhance representation learning and generalization.
 123 Predicting future states or properties over multiple steps is a powerful self-supervisory signal that
 124 encourages models to capture system dynamics and long-range dependencies. This is a common
 125 strategy in reinforcement learning (Merlis et al., 2024) and sequence modeling. In molecular modeling,
 126 while some GNNs use multi-step prediction as the primary goal for trajectory forecasting like
 127 MDNet (Zheng et al., 2021), or employ other self-supervised tasks like masked position prediction (An
 128 et al., 2025), FRAMES specifically uses a multi-step lookahead loss on future energies and forces as
 129 an auxiliary objective. The goal is to enrich the GNN’s latent representation for improved single-step
 130 prediction accuracy and efficiency, rather than direct multi-step forecasting at inference.
 131

132 Denoising-based objectives are closely related but complementary to our approach. Noisy-node style
 133 regularization (Godwin et al., 2022) perturbs equilibrium structures with small random displacements
 134 and trains the model to predict the clean configuration, and the recent DeNS method (Liao et al.,
 135 2024) applies a similar idea to non-equilibrium structures along its trajectory. These methods operate
 136 on unordered or partially ordered sets of structures and do not explicitly exploit full MD trajectories.
 137 In contrast, FRAMES leverages the temporal ordering of MD data and shows that, for the benchmarks
 138 studied here, minimal temporal context from two consecutive frames already captures most of the
 139 useful dynamical signal. We view DeNS and noisy-node-style objectives as complementary: they can
 140 be applied in settings without full trajectories and could in principle be combined with FRAMES in
 141 future work.
 142

143 FlashMD(Bigi et al., 2025) proposes direct, long-stride prediction of MD trajectories, taking as input
 144 the positions and momenta at a single time step and predicting the configuration at a later time. Their
 145 focus is on designing architectures and constraints for fast and stable multi-step MD simulation,
 146 whereas our contribution is a training strategy for static predictors that uses an auxiliary temporal
 147 loss but leaves inference purely single-frame. Conceptually, their observation that MD is effectively
 148 Markovian and can be advanced from the current state alone complements our empirical finding that
 149 a very short temporal context (two frames) already provides most of the useful dynamical signal for
 150 improving static energy/force prediction.
 151

3 METHOD

152 In §3.1, we formalize the task of energy and force prediction; in §3.2, we describe our model
 153 architecture; in §3.3, we detail the FRAMES training objective; and finally, in §3.4, we explain how
 154 this framework is used to test our hypothesis on temporal data redundancy.
 155

3.1 PROBLEM FORMALIZATION AND PROPOSED APPROACH

156 The accurate prediction of quantum mechanical properties, such as energy and forces, is essential
 157 for modeling complex atomic systems like molecules and crystals. While this paper utilizes datasets
 158 generated from Molecular Dynamics (MD) simulations, which consist of atomic trajectories, our
 159 primary goal is to enhance predictors that operate on single, static snapshots from these trajectories.
 160

162

163

Training with Auxiliary Loss

164

165

166

167

168

169

170

171

172

173

174

175

176

177

178

179

180

181

182

183

184

185

186

187

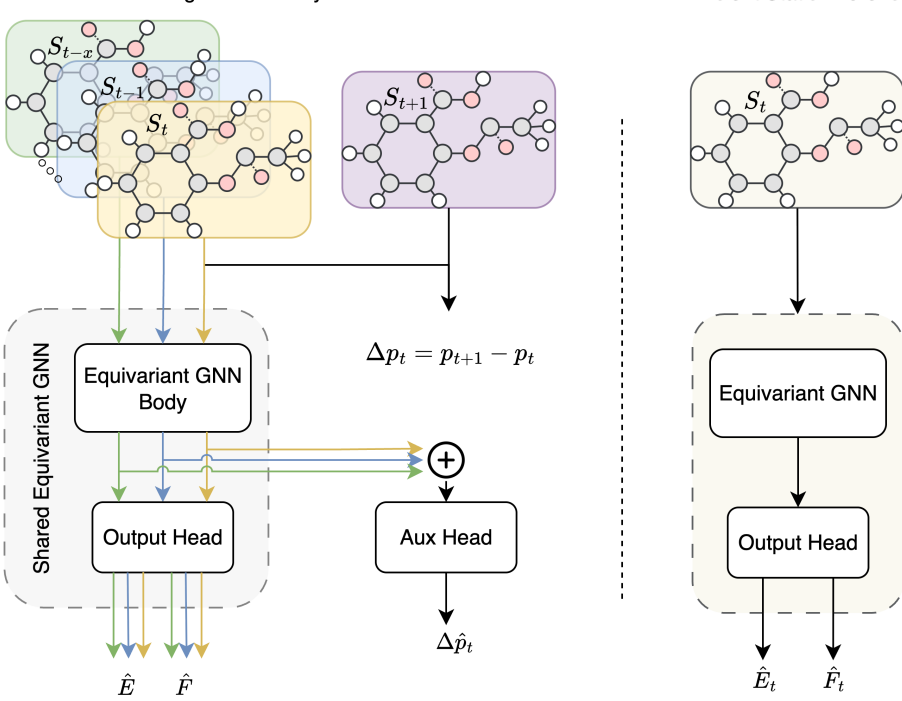


Figure 1: An overview of our proposed training and inference framework. On the left, the shared GNN body processes a history of frames (S_t, S_{t-1} , etc.) to produce latent embeddings. The primary Output Head uses these embeddings to predict energies and forces for the entire window, supervised by a primary loss. Concurrently, the embeddings are concatenated \oplus and fed to an Auxiliary Head, which is trained with an auxiliary loss to predict the displacement to the next frame Δr_t . On the right, at test time, the auxiliary head is detached. The model operates as a simple, static predictor, taking a single frame S_t as input to efficiently predict its corresponding energy and forces.

194

195

We define an atomic system’s configuration at a specific time t as a frame, S_t , represented by a set of tuples $S_t = \{(z_i, \mathbf{r}_i) \mid i = 1, \dots, m\}$ where for each of m atoms, $z_i \in \mathbb{N}$ is its atomic number and $\mathbf{r}_i \in \mathbb{R}^3$ is its 3D position vector.

196

197

Associated with each frame S_t is a scalar potential energy shown with $E_t \in \mathbb{R}$, and a set of the atom-wise forces, $F_t = \{\mathbf{f}_i \in \mathbb{R}^3 \mid i \in \{1, \dots, m\}\}$, where each f_i is the force vector acting on the i -th atom.

202

203

To avoid confusion with momentum, we use \mathbf{r} for atomic positions throughout.

204

205

Task Definition We aim to learn the function f_ϕ , parameterized by ϕ , which maps a single static frame S_t to its corresponding energy and forces. Formally, the task is:

206

207

$$f_\phi(S_t) \rightarrow \{\hat{E}_t, \hat{F}_t\} \quad (1)$$

208

where \hat{E}_t and \hat{F}_t are the model’s prediction for the true Energy and forces.

209

210

Proposed Approach Although the system configuration at any given instant determines its energy and, thereby, forces operating on each atom, the temporal evolution of the system overtime provides additional cues over the space of possible energy/force values. However, learning these spatio-temporal dynamics adds to the computational burden, given that the trajectories evolve over long time periods. Instead of relying on complex spatio-temporal models, we aim to capture the useful temporal dynamics from MD trajectories in a lightweight way, so that static predictors can benefit

216 from temporal information while still operating on single configurations at test time. The key insight
 217 is that temporal correlations contain rich cues about energy and forces, but extracting them does not
 218 require long histories. In fact, we hypothesize that minimal temporal information — such as pairs of
 219 consecutive frames — can be sufficient and likely even more effective than using longer trajectories,
 220 which often introduce redundancy and noise. In the following, we describe our model architecture.
 221

222 3.2 MODEL ARCHITECTURE

224 Our model consists of two main components: a shared GNN Backbone that processes atomic config-
 225 urations into latent representations, and two distinct Prediction Heads that use these representations
 226 to perform the primary and auxiliary tasks (Figure 1).
 227

228 3.2.1 THE GNN BACKBONE

229 For our GNN backbone, we employ Equiformer architecture (Liao & Smidt, 2023), an $E(3)$ -
 230 equivariant graph attention transformer. The function of the GNN backbone is to map a single
 231 atomic frame, S_t , into a set of rich, equivariant latent feature vectors, h_t , one for each atom in the
 232 system.
 233

234 During training, this GNN backbone is applied independently to each frame in the input window
 235 (S_{t-T+1}, \dots, S_t) with shared weights, which produces a sequence of embeddings, (h_{t-T+1}, \dots, h_t)
 236 that serves as input to the prediction heads.
 237

238 3.2.2 PREDICTION HEADS

239 The latent embeddings produced by the GNN backbone are passed to two distinct prediction heads
 240 for our multi-task objective.
 241

242 **Output Head** The Primary Head is responsible for the main prediction task. For each frame S_t
 243 in the input window, its corresponding embedding h_t is fed into the Primary Head to produce the
 244 predicted energy \hat{E}_t and forces \hat{F}_t for that specific frame. For the scalar value, energy, a feedforward
 245 network transforms embedding features h_t on each node into a scalar and then sums over all nodes.
 246 The atomic forces \hat{F}_t are then derived analytically as the negative gradient of the predicted energy
 247 with respect to the atomic positions, $\hat{F}_t = -\nabla_{\mathbf{r}_t} \hat{E}_t$, ensuring energy conservation.
 248

249 **Auxiliary Head** Used only during training, the Auxiliary Head’s role is to help the model learn
 250 from the system’s temporal dynamics.
 251

252 Unlike the Primary Head, the Auxiliary Head takes the concatenated embeddings from the entire
 253 historical window of T frames as its single input. This input is the vector $z = [h_{t-T+1}, \dots, h_t]$. It
 254 processes this concatenated vector to predict a single output: the atomic displacement to the next
 255 frame, $\Delta\hat{p}_t$.
 256

257 The Auxiliary Head is itself an equivariant graph attention network, consistent with the GNN
 258 backbone. This ensures that the processing of the concatenated temporal information respects the
 259 underlying physical symmetries of the system.
 260

261 3.3 THE FRAMES TRAINING OBJECTIVE

262 To improve the performance of the static predictor defined in §3.1, we introduce a multi-task training
 263 objective called FRAMES. This objective is used only during training and combines a standard
 264 primary loss with our novel auxiliary loss. The total loss, \mathcal{L}_{total} is a weighted sum of these two
 265 components:
 266

$$\mathcal{L}_{total} = \mathcal{L}_{primary} + \lambda_{aux} \mathcal{L}_{aux} \quad (2)$$

267 where λ_{aux} is a hyperparameter that balances the contribution of the auxiliary task. To ensure
 268 stable training, all ground-truth energy and force values are normalized before being used in the loss
 269 calculations. We now describe each component in detail.
 270

Because the FRAMES objective only augments the loss and does not constrain the backbone architecture, it is directly applicable to a wide range of MLIP models (e.g., Equiformer, NequIP, EGNN). In all experiments below we instantiate FRAMES with Equiformer, but no architectural changes are required to transfer the same objective to other backbones.

3.3.1 THE PRIMARY LOSS $\mathcal{L}_{primary}$

The primary loss, $\mathcal{L}_{primary}$ measures the accuracy of the model on the main task of predicting energy and forces. For each of the T frames in the input window, the output head produces the prediction (\hat{E}_t, \hat{F}_t) . The primary loss averages error over this entire window, which is a weighted sum of energy and force error:

$$\mathcal{L}_{primary} = \frac{1}{T} \sum_{t'=t-T+1}^t \left(\lambda_E |E_{t'} - \hat{E}_{t'}| + \lambda_F \|F_{t'} - \hat{F}_{t'}\|_2 \right) \quad (3)$$

where λ_E and λ_F are loss-weighting hyperparameters.

3.3.2 THE AUXILIARY LOSS \mathcal{L}_{aux}

The goal of our auxiliary task is to predict the atomic displacement to the next frame. We define this ground-truth displacement vector, calculated from the simulation data, as:

$$\Delta \mathbf{r}_t = \mathbf{r}_{t+1} - \mathbf{r}_t \quad (4)$$

As described in §3.2, the Auxiliary Head takes the concatenated embeddings, $z = [h_{t-T+1}, \dots, h_t]$ and outputs a single prediction of this displacement, denoted as $\Delta \hat{p}_t$. Having these two in mind, the auxiliary loss, \mathcal{L}_{aux} is defined as the L2 norm between ground-truth and predicted displacement:

$$\mathcal{L}_{aux} = \|\Delta \hat{p}_t - \Delta \mathbf{r}_t\|_2 \quad (5)$$

By encouraging the model to predict the subsequent motion from the embeddings, this auxiliary task forces the model to learn a representation that is more grounded in the system’s physical dynamics, thereby improving performance on the primary task.

Because the FRAMES objective only augments the loss and does not constrain the backbone architecture, it is directly applicable to a wide range of MLIP models (e.g., Equiformer, NequIP, EGNN). In all experiments below we instantiate FRAMES with Equiformer, but no architectural changes are required to transfer the same objective to other backbones.

3.4 INVESTIGATING TEMPORAL REDUNDANCY

Our FRAMES framework provides a controlled testbed to investigate the central hypothesis of this work: that for distilling physical priors from dynamics, minimal temporal information is optimal, and that including additional historical data can be detrimental.

To test this hypothesis, we systematically vary the number of historical frames, T , used to create the concatenated embedding $z = [h_{t-T+1}, \dots, h_t]$, for the auxiliary task. We train several otherwise identical models, each with a different value of T .

We specifically compare the following three conditions:

- **Baseline ($T = 1$):** This model is trained using only the primary loss, with no auxiliary objective. It represents a standard, purely static predictor.
- **FRAMES ($T = 2$):** Our main proposed model. The auxiliary head is trained on concatenated embeddings from two consecutive frames, providing it with information analogous to velocity.
- **FRAMES ($T = 3$):** A model trained with an auxiliary head fed embeddings from three consecutive frames, providing it with information analogous to acceleration.

324
 325 Table 1: Mean absolute error results on the MD17 testing set. Energy and force are in units of meV
 326 and meV/Å, respectively. This table compares several baseline models against our Equiformer-based
 327 approach, which is tested using both two and three frames of temporal context to investigate the
 328 effects of data redundancy.

Model	Aspirin		Benzene		Ethanol		Malonaldehyde		Naphthalene		Salicylic acid		Toluene		Uracil	
	energy	forces	energy	forces	energy	forces	energy	forces	energy	forces	energy	forces	energy	forces	energy	forces
SchNet (Schütt et al., 2017)	16.0	58.5	3.5	13.4	3.5	16.9	5.6	28.6	6.9	25.2	8.7	36.9	5.2	24.7	6.1	24.3
DimeNet (Gasteiger et al., 2020)	8.8	21.6	3.4	8.1	2.8	10.0	4.5	16.6	5.3	9.3	5.8	16.2	4.4	9.4	5.0	13.1
PaiNN (Schütt et al., 2021)	6.9	14.7	-	-	2.7	9.7	3.9	13.8	5.0	3.3	4.9	8.5	4.1	4.1	4.5	6.0
TorchMD-NET (Thölke & Fabriiis, 2022)	5.3	11.0	2.5	8.5	2.3	4.7	3.3	7.3	3.7	2.6	4.0	5.6	3.2	2.9	4.1	4.1
NequIP ($L_{max} = 3$) (Batzner et al., 2022)	5.7	8.0	-	-	2.2	3.1	3.3	5.6	4.9	1.7	4.6	3.9	4.0	2.0	4.5	3.3
Equiformer	5.3	7.2	2.2	6.6	2.2	3.1	3.3	5.8	3.7	2.1	4.5	4.1	3.8	2.1	4.3	3.8
Equiformer+Noisy Nodes	10.5	8	4.3	6.3	2.6	3.8	3.6	6.3	3.6	2.5	6	5.2	4.3	2.3	6.5	5.5
Equiformer + 2 Frames	5.2 _{±0.16}	7.0 _{±0.09}	2.4 _{±0.07}	6.3 _{±0.27}	2.2 _{±0.02}	3.2 _{±0.05}	3.3 _{±0.05}	5.6 _{±0.17}	3.6 _{±0.03}	2.2	4.3 _{±0.25}	4.1 _{±0.04}	3.6 _{±0.03}	2 _{±0.09}	4.1 _{±0.12}	3.5 _{±0.10}
Equiformer + 3 Frames	5.3	7.3	2.6	6.1	2.2	3.5	3.3	6	3.8	2.4	4.4	4.4	3.5	2	4.1	3.9

335 Crucially, while the models are trained differently, they are all evaluated on the exact same task at
 336 inference time: the accuracy of static energy and force prediction on the test set, using only a single
 337 frame S_t as input. The performance on this final task will be used to validate our hypothesis.

339 To ensure a fair and controlled comparison, all other aspects of the experimental setup are held
 340 constant across these cases. This includes the core model architecture, the training objective (the
 341 combined primary and auxiliary loss function), and all hyperparameters.

4 EXPERIMENTS

345 To validate our proposed FRAMES framework and test our hypothesis on temporal data redundancy,
 346 we conduct a series of experiments on standard benchmarks. We begin in §4.1 by evaluating our
 347 primary results on the widely-used MD17 dataset, comparing our method against several state-of-
 348 the-art baselines. Then in §4.1 we present a key ablation study to justify our choice of auxiliary
 349 objective. Finally, we test the generalization of our findings on the ISO17 dataset in §4.2 and
 350 provide an illustrative example on a spring-mass system in §4.3 which helps provide insights into the
 351 phenomenon.

4.1 MD17 DATASET

354 **Dataset.** The MD17 dataset (Chmiela et al., 2017) features ab-initio molecular dynamics trajectories
 355 for 8 small organic molecules, including Aspirin and Toluene. The primary task is to predict the
 356 potential energy and inter-atomic forces for each molecular configuration (frame) in a trajectory.
 357 Following standard benchmarks, we use 950 frames for training and 50 for validation, with the
 358 remainder used for testing. Crucially for our temporal analysis, we ensure that training samples are
 359 drawn sequentially with a fixed time lag of Δ_t between them, preserving the physical dynamics of
 360 the original simulation.

361 **Implementation details.** We train Equiformer (Liao & Smidt, 2023) with FRAMES based on the
 362 official implementation. We trained this model once with two frames as input, and once with three
 363 frames as input. **We also implemented a noisy-node style auxiliary loss, where the model predicts
 364 atomic displacements from small random perturbations of the current structure, and considered it as
 365 another usefull baseline. Further details of the noisy-node baseline are provided in Appendix A.5.**

367 **Main Results.** The results, presented in Table 1, strongly support our central hypothesis. The
 368 *Equiformer + 2 Frames* model, which is supplied with velocity information, consistently outperforms
 369 the standard *Equiformer* ($T = 1$) baseline across nearly all molecules, achieving the best force
 370 prediction on 5 out of 8 molecules. In contrast, the *Equiformer + 3 Frames* model, which implicitly
 371 includes acceleration data, shows a marked degradation in performance. For instance, in molecules
 372 like Benzene and Malonaldehyde, its performance on force prediction is worse than the $T = 2$ model
 373 and is comparable or worse than the $T=1$ baseline. This trend suggests that adding further temporal
 374 context beyond velocity introduces redundant information, which, akin to multicollinearity, hinders
 375 the model’s ability to learn the underlying force field effectively.

376 **Ablation Study.** We conducted an ablation study to empirically validate our choice of the auxiliary
 377 learning objective, as defined in §3.3. We compare two distinct auxiliary loss formulations for

378 our FRAMES (T=2) model. The first is our proposed method, which uses a loss on the predicted
 379 displacement, $\mathcal{L}_{aux} = \|\Delta\hat{p}_t - \Delta\mathbf{r}_t\|_2$. The second is a more conventional alternative, which uses a
 380 loss on the predicted energy and forces of the next frame, $\mathcal{L}'_{aux} = \lambda_E|E_{t+1} - \hat{E}_{t+1}| + \lambda_F\|F_{t+1} -$
 381 $\hat{F}_{t+1}\|_2$.
 382

383 The results, presented in Table 2, show that both objectives provide a significant improvement over the
 384 baseline, with highly competitive overall performance. While predicting future forces and energies
 385 yields marginally better results on some molecules (e.g., Benzene), our proposed displacement
 386 prediction objective achieves superior or equivalent performance on the majority of the benchmark,
 387 including on larger molecules like Aspirin and Salicylic Acid.
 388

389 Given that displacement prediction offers more consistent performance across the benchmark and
 390 represents a more direct and fundamental dynamic property (the immediate consequence of the
 391 current frame’s forces), we confirm its effectiveness and select it as the default auxiliary objective for
 392 our FRAMES framework.
 393

394 Table 2: Ablation study on the choice of auxiliary loss for the $T = 2$ model. We compare our proposed
 395 method, which uses a loss on atomic displacements (Aux: E_{t+1}, F_{t+1}) against our proposed method
 396 of predicting atomic displacements (Aux: $\Delta\mathbf{r}_t$). Results are mean absolute error (MAE) in meV for
 397 energy and meV/Å for forces.
 398

Model (T=2)	Aspirin		Benzene		Ethanol		Malonaldehyde		Naphthalene		Salicylic acid		Toluene		Uracil	
	energy	forces	energy	forces	energy	forces	energy	forces	energy	forces	energy	forces	energy	forces	energy	forces
Equiformer (T=1, Baseline)	5.3	7.2	2.2	6.6	2.2	3.1	3.3	5.8	3.7	2.1	4.5	4.1	3.8	2.1	4.3	3.8
FRAMES (T=2) with Aux: E_{t+1}, F_{t+1}	5.3	7.2	2.3	6.1	2.2	3.2	3.2	5.6	3.6	2.2	4.4	4.2	3.8	1.9	4.1	3.6
FRAMES (T=2) with Aux: $\Delta\mathbf{r}_t$	5.2	7.0	2.4	6.3	2.2	3.2	3.3	5.6	3.6	2.2	4.3	4.1	3.6	2.0	4.2	3.5

401 4.2 ISO17 DATASET

402 **Dataset.** We further validate our approach on the ISO17 dataset (Schütt et al., 2017). This dataset
 403 contains molecular dynamics trajectories of 129 isomers of $C_7O_2H_{10}$, presenting a different challenge
 404 by testing generalization across constitutional isomers. As described in the original work, the dataset
 405 is split into two evaluation scenarios. The first, which we term “Within Distribution,” tests for
 406 generalization to unseen conformations of molecules that were included in the training set. The
 407 second, more challenging “Outside Distribution” scenario tests for generalization to entirely new
 408 molecular structures (isomers) that the model has never seen during training.
 409

410 **Results.** The results, presented in Table 3, demonstrate the remarkable generalization capability of
 411 our FRAMES framework. Our FRAMES (T=2) model achieves the best performance by a significant
 412 margin across all four evaluation metrics. On the “Within Distribution” task, it substantially improves
 413 upon the baseline, confirming that our method learns a more accurate potential energy surface. More
 414 importantly, on the challenging “Outside Distribution” task, FRAMES (T=2) shows a dramatic
 415 improvement in generalizing to unseen isomers, indicating that the physical priors learned via the
 416 auxiliary loss are not molecule-specific. Consistent with our findings on MD17, the FRAMES
 417 (T=3) model shows a clear degradation in performance, often performing worse than the baseline.
 418 This validates our central hypothesis that minimal temporal information is optimal and that data
 419 redundancy hinders generalization, even across different chemical structures.
 420

421 4.3 SPRING-MASS

422 To build intuition for our hypothesis, we analyze a simple spring–mass system where the underlying
 423 physics is known. This toy problem allows us to create a controlled environment to illustrate the
 424 effects of data redundancy when predicting forces (equivalently, accelerations since $m=1$) from
 425 trajectory data, a scenario directly analogous to the multicollinearity problem in linear regression.
 426 We test both a simple linear regressor and a non–linear predictor on this problem to demonstrate
 427 how redundant temporal information affects both direct estimation and more complex representation
 428 learning.
 429

430 **Implementation.** We simulate a simple harmonic oscillator governed by Hooke’s Law, $F = -kx$,
 431 setting mass $m = 1.0$ and spring constant $k = 1.0$. The trajectory is generated by numerically

432 Table 3: Mean Absolute Error on the ISO17 test sets. Our FRAMES (T=2) model is compared
 433 against the baseline Equiformer and a T=3 model. Within Distribution tests generalization to new
 434 conformations of known molecules, while Outside Distribution tests generalization to entirely new
 435 isomers.

	Within Distribution		Outside Distribution	
	Energy	Forces	Energy	Forces
Equiformer (Baseline)	0.13228	<u>0.0093</u>	0.1460	<u>0.0174</u>
FRAMES ($T = 2$)	0.00569	0.0053	0.0248	0.0154
FRAMES ($T = 3$)	<u>0.07009</u>	0.0101	<u>0.0639</u>	0.0187

444 integrating the equation of motion $\ddot{x} = -x$ to produce a time series of positions $\{\mathbf{r}_t\}$. Since $m=1$,
 445 the force and acceleration coincide, so predicting F_t is equivalent to predicting the acceleration.

446 For this synthetic dataset, we consider two simplified models: a linear model and a non-linear MLP.
 447 We randomly sample from the trajectories generated according to the above setting, and train on 8000
 448 samples for the non-linear model and 100 samples for the linear model, with 2000 samples reserved
 449 for testing.

450 The *linear model* consists of a single shared linear layer followed by two linear heads: a main
 451 head that predicts the target force F_t and an auxiliary head that predicts the FRAMES objective,
 452 the next-step displacement $\Delta\mathbf{r}_i$. The *non-linear model* has the same structure (shared body, main
 453 head, auxiliary head), but each component is implemented as a small Multi-Layer Perceptron (MLP)
 454 instead of a single linear layer.

455 For $T = 1$, the baseline, we disable the auxiliary head and train both models only with the primary
 456 loss on the current force F_t , which corresponds to a standard static predictor without FRAMES.
 457 For $T > 1$, both models are trained using the FRAMES objective. The input for a history of T is
 458 the vector of positions $[\mathbf{r}_{t-T+1}, \dots, \mathbf{r}_t]$. The primary task for both models is to predict the force
 459 F_t at the current time. For the auxiliary task, a simple linear head takes the concatenated hidden
 460 layer representations (embeddings) from the historical window and is trained to predict the next-step
 461 displacement, $\Delta\mathbf{r}_t = \mathbf{r}_{t+1} - \mathbf{r}_t$.

462 **Results.** The results, for the nonlinear model is summarized in Table 4 and for the linear model
 463 visualized in Figure 2, which both of them clearly support our central hypothesis. Performance
 464 is extremely poor with one frame ($T = 1$), as a single position does not contain information on
 465 temporal dynamics. The error decreases significantly for the ($T = 2$) model, which can infer the
 466 velocity, but increases again for ($T = 3$). This suggests that while minimal temporal information is
 467 highly beneficial, additional frames introduce redundancy that degrades performance. This simple
 468 example confirms the core principle that "less is more," that we also observe in our main experiments
 469 on complex molecular systems.

470 Table 4: Mean Squared Error (MSE) on the spring-mass toy example. T denotes the number of
 471 historical frames used as input to predict the current force.

Model	T=1	T=2	T=3	T=4	T=5	T=6
MLP Model (10^{-9})	1.24 ± 1.02	0.83 ± 0.44	1.55 ± 1.09	1.28 ± 0.72	2.15 ± 1.38	1.05 ± 0.45

479 5 CONCLUSION

480 In this work, we addressed the challenge of improving molecular force and energy prediction by
 481 leveraging temporal information from Molecular Dynamics simulations. We introduced FRAMES, a
 482 novel and model-agnostic auxiliary loss that distills physical priors from pairwise frame dynamics
 483 into a predictor that remains purely static and efficient at inference time. Our experiments on the
 484 MD17 and ISO17 benchmarks demonstrate that FRAMES significantly improves the accuracy of a
 485 strong Equiformer baseline, achieving highly competitive results in both energy and force prediction.

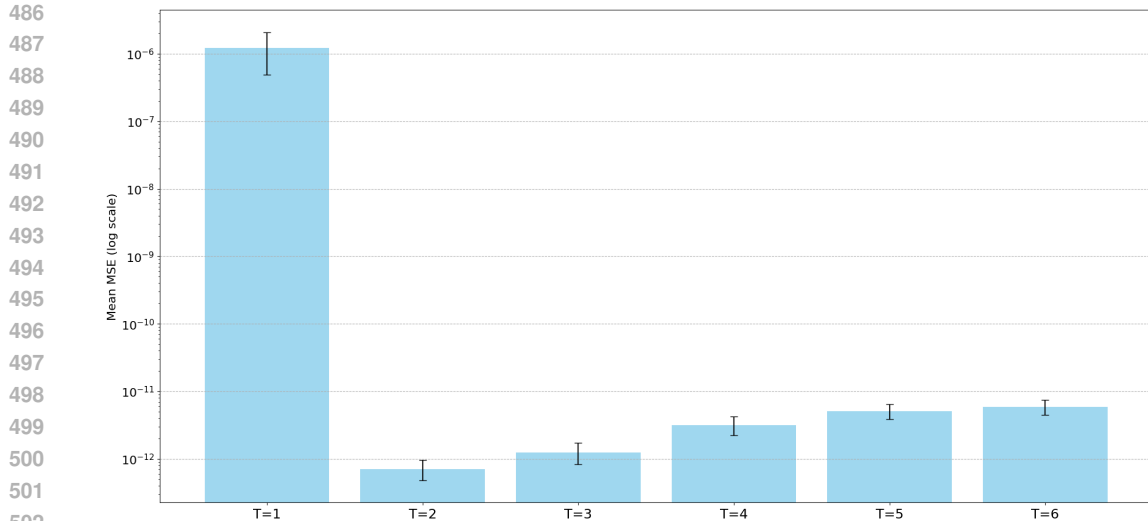


Figure 2: Mean squared error (MSE) of the linear predictor on the spring–mass toy system as a function of the history length T (x-axis). The plot highlights the large performance improvement when moving from $T=1$ to $T=2$, followed by degradation once redundant temporal information ($T \geq 3$) is included. A 95% confidence interval is shown.

Furthermore, we provided strong empirical evidence for our "less is more" hypothesis. We showed that using minimal temporal information from two consecutive frames is optimal for this task, while including more historical data in the training procedure can be detrimental, degrading model performance due to data redundancy. This finding was validated across complex molecular benchmarks and an intuitive spring–mass toy example.

Future work could explore the application of the FRAMES objective to a wider range of equivariant architectures and other scientific domains where simulation trajectories are available. Ultimately, our work highlights a simple, powerful, and computationally efficient strategy for creating more physically-grounded and accurate molecular predictors.

ETHICS STATEMENT

This work proposes a training strategy for graph neural networks aimed at improving energy and force prediction in atomic and molecular systems. The research is entirely computational and does not involve human subjects, personal data, or sensitive information. The datasets used (e.g., MD17, ISO17) are publicly available and widely adopted benchmarks in the community. We believe that the outcomes of this work will have positive impacts by advancing the use of AI for scientific discovery, particularly in molecular modeling and materials design. We do not foresee significant risks of misuse or negative societal impacts beyond those already inherent to general machine learning research in molecular simulations.

REPRODUCIBILITY STATEMENT

We have taken several steps to ensure the reproducibility of our work. Details of the FRAMES datasets and implementation details are described in the main text in Section 4, with further training hyperparameters details provided in the Appendix 5. We include results across multiple random seeds to demonstrate stability, and ablation studies to clarify the contribution of individual components. To facilitate replication, we have released anonymized source code and scripts for training and evaluation here <https://anonymous.4open.science/r/FRAMES-7AB9/README.md>.

540 REFERENCES
541

542 Junyi An, Chao Qu, Yun-Fei Shi, XinHao Liu, Qianwei Tang, Fenglei Cao, and Yuan Qi. Equivariant
543 masked position prediction for efficient molecular representation. In *International Conference*
544 *on Learning Representations (ICLR)*, 2025. URL <https://openreview.net/forum?id=Nue5iMj8n6>.

545

546 Simon Batzner, Albert Musaelian, Lixin Sun, Mario Geiger, Jonathan P. Mailoa, Mordechai Ko-
547 rnbluth, Nicola Molinari, Tess E. Smidt, and Boris Kozinsky. E(3)-equivariant graph neural
548 networks for data-efficient and accurate interatomic potentials. *Nature Communications*, 13
549 (1), May 2022. doi: 10.1038/s41467-022-29939-5. URL <https://doi.org/10.1038/s41467-022-29939-5>.

550

551 Filippo Bigi, Sanggyu Chong, Agustinus Kristiadi, and Michele Ceriotti. FlashMD: long-stride,
552 universal prediction of molecular dynamics. In *Advances in Neural Information Processing Systems*
553 (*NeurIPS*), 2025.

554

555 Lowik Chanussot, Abhishek Das, Siddharth Goyal, Thibaut Lavril, Muhammed Shuaibi, Morgane
556 Riviere, Kevin Tran, Javier Heras-Domingo, Caleb Ho, Weihua Hu, Aini Palizhati, Anuroop
557 Sriram, Brandon Wood, Junwoong Yoon, Devi Parikh, C. Lawrence Zitnick, and Zachary Ulissi.
558 Open catalyst 2020 (oc20) dataset and community challenges. *ACS Catalysis*, 2021.

559

560 Stefan Chmiela, Alexandre Tkatchenko, Huziel E. Saucedo, Igor Poltavsky, Kristof T. Schütt, and
561 Klaus-Robert Müller. Machine learning of accurate energy-conserving molecular force fields.
562 *Science Advances*, 2017.

563

564 Anders S Christensen and O Anatole von Lilienfeld. On the role of gradients for machine learning of
565 molecular energies and forces. *Machine Learning: Science and Technology*, 2020.

566

567 Alexandre Duval, Victor Schmidt, Alex Hernández-García, Santiago Miret, Fragkiskos D. Malliaros,
568 Yoshua Bengio, and David Rolnick. Faenet: Frame averaging equivariant gnn for materials
569 modeling. In *International Conference on Machine Learning (ICML)*, 2023.

570

571 Marc Finzi, Samuel Stanton, Pavel Izmailov, and Andrew Gordon Wilson. Generalizing convolutional
572 neural networks for equivariance to lie groups on arbitrary continuous data. In *International*
573 *Conference on Machine Learning*, pp. 3165–3176. PMLR, 2020.

574

575 Fabian Fuchs, Daniel E. Worrall, Volker Fischer, and Max Welling. Se(3)-transformers: 3d roto-
576 translation equivariant attention networks. In *Advances in Neural Information Processing Systems*
577 (*NeurIPS*), 2020.

578

579 Victor Garcia Satorras, Emiel Hoogeboom, Fabian Fuchs, Ingmar Posner, and Max Welling. E(n)
580 equivariant normalizing flows. In *Advances in Neural Information Processing Systems (NeurIPS)*,
581 2021.

582

583 Johannes Gasteiger, Janek Groß, and Stephan Günnemann. Directional message passing for molecular
584 graphs. In *International Conference on Learning Representations (ICLR)*, 2020. URL <https://openreview.net/forum?id=B1eWbxStPH>.

585

586 Jonathan Godwin, Michael Schaarschmidt, Alexander L Gaunt, Alvaro Sanchez-Gonzalez, Yulia
587 Rubanova, Petar Veličković, James Kirkpatrick, and Peter Battaglia. Simple GNN regularisation
588 for 3d molecular property prediction and beyond. In *International Conference on Learning*
589 *Representations (ICLR)*, 2022.

590

591 Jiaqi Han, Yu Rong, Tingyang Xu, and Wenbing Huang. Geometrically equivariant graph neural
592 networks: A survey. *arxiv preprint arXiv:2202.07230*, 2022.

593

594 Wenbing Huang, Jiaqi Han, Yu Rong, Tingyang Xu, Fuchun Sun, and Junzhou Huang. Equivariant
595 graph mechanics networks with constraints, 2022.

596

597 Michael Hutchinson, Charline Le Lan, Sheheryar Zaidi, Emilien Dupont, Yee Whye Teh, and Hyunjik
598 Kim. Lietransformer: Equivariant self-attention for lie groups. In *International Conference on*
599 *Machine Learning (ICML)*, 2021a.

594 Michael J Hutchinson, Charline Le Lan, Sheheryar Zaidi, Emilien Dupont, Yee Whye Teh, and
 595 Hyunjik Kim. Lietransformer: Equivariant self-attention for lie groups. In *International Conference*
 596 *on Machine Learning*, pp. 4533–4543. PMLR, 2021b.

597

598 Yi-Lun Liao and Tess Smidt. Equiformer: Equivariant graph attention transformer for 3d atomistic
 599 graphs. In *International Conference on Learning Representations (ICLR)*, 2023. URL <https://openreview.net/forum?id=KwmPfARgOTD>.

600

601 Yi-Lun Liao, Tess Smidt, Muhammed Shuaibi, and Abhishek Das. Generalizing denoising to
 602 non-equilibrium structures improves equivariant force fields. *Transactions on Machine Learning*
 603 *Research (TMLR)*, 2024.

604

605 Nadav Merlis, Dorian Baudry, and Vianney Perchet. The value of reward lookahead in reinforcement
 606 learning. In *Advances in Neural Information Processing Systems (NeurIPS)*, 2024. URL <https://openreview.net/forum?id=URyeU8mwz1>.

607

608 Víctor Garcia Satorras, Emiel Hoogeboom, and Max Welling. E(n) equivariant graph neural networks.
 609 In *International Conference on Machine Learning (ICML)*, 2021a.

610

611 Víctor Garcia Satorras, Emiel Hoogeboom, and Max Welling. E (n) equivariant graph neural networks.
 612 In *International conference on machine learning*, pp. 9323–9332. PMLR, 2021b.

613

614 K. T. Schütt, P.-J. Kindermans, H. E. Saucedo, S. Chmiela, A. Tkatchenko, and K.-R. Müller. Schnet:
 615 A continuous-filter convolutional neural network for modeling quantum interactions. In *Advances*
 616 *in Neural Information Processing Systems (NeurIPS)*, 2017.

617

618 Kristof T. Schütt, Oliver T. Unke, and Michael Gastegger. Equivariant message passing for the
 619 prediction of tensorial properties and molecular spectra. In *International Conference on Machine*
 620 *Learning (ICML)*, 2021.

621

622 Philipp Thölke and Gianni De Fabritiis. Equivariant transformers for neural network based molecular
 623 potentials. In *International Conference on Learning Representations (ICLR)*, 2022. URL <https://openreview.net/forum?id=zNHzqZ9wrRB>.

624

625 Nathaniel Thomas, Tess E. Smidt, Steven Kearnes, Lusann Yang, Li Li, Kai Kohlhoff, and Patrick
 626 Riley. Tensor field networks: Rotation- and translation-equivariant neural networks for 3d point
 627 clouds. *arxiv preprint arXiv:1802.08219*, 2018.

628

629 Richard Tran, Janice Lan, Muhammed Shuaibi, Brandon M. Wood, Siddharth Goyal, Abhishek Das,
 630 Javier Heras-Domingo, Adeesh Kolluru, Ammar Rizvi, Nima Shoghi, Anuroop Sriram, Félix
 631 Therrien, Jehad Abed, Oleksandr Voznyy, Edward H. Sargent, Zachary Ulissi, and C. Lawrence
 Zitnick. The open catalyst 2022 (oc22) dataset and challenges for oxide electrocatalysts. *ACS*
 632 *Catalysis*, 2023.

633

634 Liming Wu, Zhichao Hou, Jirui Yuan, Yu Rong, and Wenbing Huang. Equivariant spatio-temporal
 635 attentive graph networks to simulate physical dynamics. In *Advances in Neural Information*
 636 *Processing Systems (NeurIPS)*, 2023. URL <https://openreview.net/forum?id=35nFSbEBks>.

637

638 Zonghan Wu, Shirui Pan, Fengwen Chen, Guodong Long, Chengqi Zhang, and S Yu Philip. A
 639 comprehensive survey on graph neural networks. *IEEE transactions on neural networks and*
 640 *learning systems*, 32(1):4–24, 2020.

641

642 Minkai Xu, Jiaqi Han, Aaron Lou, Jean Kossaifi, Arvind Ramanathan, Kamyar Azizzadenesheli,
 643 Jure Leskovec, Stefano Ermon, and Anima Anandkumar. Equivariant graph neural operator for
 644 modeling 3d dynamics. *arXiv preprint arXiv:2401.11037*, 2024.

645

646 Tianze Zheng, Weihao Gao, and Chong Wang. Learning large-time-step molecular dynamics
 647 with graph neural networks. In *NeurIPS 2021 AI for Science Workshop*, 2021. URL <https://openreview.net/forum?id=cmXGBW7hN6Q>.

648

649

648 **A APPENDIX: EXPERIMENTAL DETAILS**
649650 Our implementation is based on the official open-source code for Equiformer (Liao & Smidt, 2023).
651 For hyperparameters shared with the original work, we adopt their reported values unless otherwise
652 specified to ensure a fair comparison. All models were trained using an Adam optimizer with an
653 initial learning rate of 5×10^{-4} .
654655 **A.1 TRAINING PROCEDURE**
656657 For the FRAMES models, the auxiliary loss weight, λ_{aux} , was linearly decayed from its initial value
658 (see Table 5) to 0 over the course of training. To manage the memory requirements of processing
659 historical data, we adjusted the batch sizes. The baseline model ('T=1') used a batch size of 8. For
660 **FRAMES**, we used a batch size of 4 for both the 'T=2' and 'T=3' configurations.
661662 **A.2 TRAJECTORY SUBSAMPLING FOR MD EXPERIMENTS**
663664 For all MD-based experiments (MD17 and ISO17), we do not feed every raw MD frame directly to
665 the model. Instead, for each molecule we construct shorter sub-trajectories by uniformly subsampling
666 frames along the original trajectory. Let (S_1, \dots, S_L) denote the sequence of configurations for a
667 given molecule. We choose a stride $k \geq 1$ and build training windows of length T as
668

669
$$(S_t, S_{t+k}, S_{t+2k}, \dots, S_{t+(T-1)k}),$$

670

671 so that consecutive frames inside a window are equally spaced and separated by k steps in the original
672 MD trajectory. The stride k is chosen automatically for each trajectory based on its length and the
673 desired number of training samples, so that we obtain approximately the target number of windows
674 while keeping the frames in each window well separated (typically on the order of tens of MD steps).
675676 Note that although the frames in a sub-trajectory are non-adjacent in the original MD sequence when
677 $k > 1$, the FRAMES auxiliary target is always defined on adjacent elements of the *subsampled*
678 window. Concretely, if (S_t, S_{t+k}, \dots) is a window, we predict the displacement $\Delta r_j = r_{j+1} - r_j$
679 between consecutive frames inside this subsampled sequence, where r_j and r_{j+1} correspond to
680 configurations that are k integration steps apart in the underlying MD trajectory.
681682 **A.3 MD17 HYPERPARAMETERS**
683684 The key loss coefficients for our experiments on the MD17 dataset are detailed in Table 5.
685686 **Table 5:** Hyperparameters used for training our 'FRAMES' models on the MD17 dataset. We report
687 the coefficients for the primary loss (λ_E, λ_F) and the initial value for the auxiliary loss (λ_{aux}).
688

Hyper-parameter	Aspirin	Benzene	Ethanol	Malonaldehyde	Naphthalene	Salicylic acid	Toluene	Uracil
Energy coefficient λ_E	1	1	1	1	2	1	1	1
Force coefficient λ_F	80	80	80	100	20	80	80	20
FRAMES coefficient λ_{aux}	1	0.25	0.25	0.25	1	1	1	0.25

690 **A.4 ISO17 HYPERPARAMETERS**
691692 For the ISO17 experiments, we used a consistent set of hyperparameters across all isomers: the
693 energy coefficient $\lambda_E = 1$, the force coefficient $\lambda_F = 80$, and the initial auxiliary loss coefficient
694 $\lambda_{aux} = 0.25$. The model architecture and training procedure were kept identical to those used for the
695 MD17 experiments.
696697 **A.5 NOISY-NODE AUXILIARY OBJECTIVE**
698699 For the noisy-node baseline, we follow the general idea of Godwin et al. (2022) and add an additional
700 denoising-style auxiliary loss on top of the main energy/force prediction loss. Concretely, during
701 training we apply the following procedure independently for each graph (configuration): with
702 probability $p_{noise} = 0.1$ we construct a corrupted version of the input by randomly selecting a
703

702 fraction $p_{\text{corr}} = 0.25$ of the atoms and perturbing their positions with small Gaussian noise of
 703 standard deviation 0.02 (in the same units as the input coordinates). The backbone GNN encodes this
 704 corrupted structure, and an auxiliary head is trained to predict the displacement between the clean
 705 and noisy positions (i.e., to denoise the perturbed atoms). The auxiliary noisy-node loss is combined
 706 with the main loss using a fixed weight $\lambda_{\text{aux}} = 5$, so that the total objective is

$$707 \quad 708 \quad L_{\text{total}} = L_{\text{main}} + \lambda_{\text{aux}} L_{\text{noisy-node}}.$$

709 This auxiliary head is used only during training; at inference time the model reduces to the standard
 710 single-frame predictor without any denoising branch.

711
 712
 713
 714
 715
 716
 717
 718
 719
 720
 721
 722
 723
 724
 725
 726
 727
 728
 729
 730
 731
 732
 733
 734
 735
 736
 737
 738
 739
 740
 741
 742
 743
 744
 745
 746
 747
 748
 749
 750
 751
 752
 753
 754
 755